Journal of Molecular Graphics and Modelling 29 (2011) 975–984

Contents lists available at ScienceDirect

Journal of Molecular Graphics and Modelling

journal homepage: www.elsevier.com/locate/JMGM

The effects of amino-acid mutations on specific interactions between urokinase-type plasminogen activator and its receptor: *Ab initio* molecular orbital calculations

Shingo Tsuji[a], Tomoyo Kasumi[a], Keisuke Nagase[a], Eri Yoshikawa[a], Hiroshi Kobayashi[b], Noriyuki Kurita[a,*]

[a] *Department of Computer Science and Engineering, Toyohashi University of Technology, Tempaku-cho, Toyohashi, Aichi 441-8580, Japan*
[b] *Department of Obstetrics and Gynecology, Nara Medical University, 840 Shijo-cho, Kashihara, Nara 634-8521, Japan*

ARTICLE INFO

Article history:
Received 27 December 2010
Received in revised form 7 April 2011
Accepted 7 April 2011
Available online 16 April 2011

Keywords:
Cancer metastasis
Cancer invasion
Urokinase-type plasminogen activator
Urokinase receptor
Molecular mechanics simulation
Fragment molecular orbital method
Molecular orbital calculation
Specific interaction
Protein–protein interaction
Antagonist

ABSTRACT

During cancer invasion, the binding of urokinase-type plasminogen activator (uPA) to its receptor (uPAR) on the surface of a cancer cell is considered a trigger for invasion. Here, we present a stable structure of the solvated complex formed between uPA and uPAR (uPA–uPAR) and investigate the specific interactions between uPA and uPAR by *ab initio* fragment molecular orbital (FMO) calculations. The result indicates that the electrostatic interactions between the charged amino acid residues existing in both uPA and uPAR make a large contribution to the binding between uPA and uPAR. In particular, Lys23, Lys46, Lys98 and Lys61 of uPA are found to have strong attractive interactions with uPAR. To elucidate the effect of these residues on the interactions between uPA and uPAR, we substituted each of them with the uncharged amino acid Leu and investigated the interactions between the mutated uPA and wild-type uPAR. The interaction energies indicate that Lys46 and Lys98, which bind uPA to the rim of the central ligand-binding cavity of uPAR, make greater contributions to the binding between uPA and uPAR than Lys23, which is positioned at the bottom of the ligand-binding cavity of uPAR. The effect of hydrating water molecules located between uPA and uPAR is also investigated to be significant for the specific interactions between uPA and uPAR. These results are expected to be informative for developing new peptide antagonists that block the binding of uPA to uPAR.

1. Introduction

The number of diagnosed deaths due to cancer has been steadily increasing. Cancer cells can spread within internal organs of the body by metastasis and quickly proliferate, leading to a decrease in the number of healthy cells. Finally, cancer patients lose vital body functions, leading to death. If cancer metastasis could be inhibited, it is expected that the recovery rate for cancer patients would rapidly improve. Thus, it is necessary to develop medicines that suppress cancer metastasis. These medicines are usually administered to cancer patients after removing cancerous tumors by surgery. After surgery, cancer patients have such diminished physical strength that they cannot tolerate medicines with strong side effects such as is typical of anti-cancer agents. Therefore, it is essential to develop medicines with relatively few side effects [1].

During the processes of invasion and metastasis, cancer cells produce various proteases to dissolve cell tissues such as extracellular matrix (ECM) and basement membrane and to facilitate invasion into blood vessels. The cancer cell passes through the blood vessel to reach the endothelial cells of other organs and invades these cells to develop a new metastatic focus [2]. By repeating this process, cancer cells grow proliferously. The inhibition of cancer invasion is expected to suppress cancer metastasis, resulting in good prognoses for the cancer patients.

Recent biochemical experiments have elucidated many types of proteases playing essential roles in the invasion mechanism of cancer cells [3]. Among these proteases, urokinase-type plasminogen activator (uPA) [4,5] has been found to play a key role in cancer invasion and metastasis. The specific binding of the amino-terminal fragment (ATF) of uPA to the uPA receptor (uPAR) existing on the surface of cancer cells is considered a trigger for promoting cancer invasions. The cancer cells assemble uPARs in direction they are moving and bind uPA to uPAR. The uPA that is bound to uPAR efficiently converts inactive plasminogen existing on the surface of cancer cells into the active serine protease plasmin, which directly or indirectly dissolves ECM components [6]. Therefore, blocking uPA–uPAR binding is expected to inhibit cancer invasions. Based on this idea, Kobayashi et al. synthesized the chimeric protein ATF-HI-

* Corresponding author. Tel.: +81 532 44 6875; fax: +81 532 44 6875.
E-mail address: kurita@cs.tut.ac.jp (N. Kurita).

1093-3263/$ – see front matter © 2011 Elsevier Inc. All rights reserved.
doi:10.1016/j.jmgm.2011.04.003

Table 1
Amino acid residues of uPAR missing in each PDB structure.

PDB ID	3BT1	3LAQ	2FD6	2I9B (monomer 1, 2)
Missing amino acid residues of uPAR	83–84	82–92 227–231	81–91 130–139 249–251	106–109 132–136 246–249

8 [7], which is composed of bikunin, found in amniotic fluid, and the ATF of uPA. The effectiveness of this chimeric protein on inhibiting cancer invasion has been confirmed by the biological studies using laboratory animals [1]. Recently, we [8,9] obtained stable structures of ATF-HI-8 in water and investigated their electronic properties using semiempirical molecular orbital (MO) calculations. Based on the computed results, we have proposed parts of ATF-HI-8 that are important for the specific interactions between ATF-HI-8 and uPAR.

In previous structural analyses [10,11] of the complex between uPA and uPAR, it was elucidated that the ATF of uPA, which is composed of amino acids 1–132 of uPA, binds specifically to uPAR. In particular, the Ω-loop (residues 19–31) of ATF was found to be responsible for the high-affinity interactions between uPA and uPAR [12]. In our previous molecular simulations [13], the specific interactions between uPA and uPAR were investigated using *ab initio* MO calculations based on the fragment MO (FMO) method [14–17].

In the present study, we have built upon our previous study [13] to obtain stable calculated structures of the solvated uPA–uPAR complex using different experimental structures to confirm the adequacy of the present molecular simulations. From the obtained interaction energies, the amino acid residues of uPA that are important for the specific interactions between uPA and uPAR have been elucidated. Furthermore, some of these important residues of uPA are mutated, and the change in the specific interactions between uPA and uPAR induced by the mutations are investigated using the *ab initio* FMO calculations. From the computed results, we attempt to propose peptides that can bind specifically to the uPA-binding site of uPAR and efficiently inhibit cancer invasion and metastasis.

2. Details of molecular simulations

2.1. Construction and optimization of a solvated structure of the uPA–uPAR complex

Four structures of the uPA–uPAR complex are registered in the Protein Data Bank (PDB). In these structures, the positions of some amino acid residues cannot be observed. Table 1 lists the missing amino acid residues in each PDB structure. In our previous simulations [13], the X-ray crystal structure with PDB ID 2I9B was employed. For our current calculations, we have employed the newest X-ray structure with PDB ID 3BT1 [18] because this structure is only missing two amino acids 83 and 84 in uPAR. This structure is of uPAR (residues 1–275) in complex with the ATF (residues 8–132) of uPA, vitronectin and other co-factors. The experiment [18] indicates that there is no direct contact between uPA and vitronectin and that the structure of the uPA–uPAR interface is not perturbed by the binding of vitronectin. Thus, we extracted the uPA–uPAR structure from this PDB structure. In addition, by using the homology modeling program SWISS-MODEL [19], we predicted the structures of these missing residues and added them into the PDB file to obtain an initial structure for the complete uPA–uPAR complex.

The N- and C-termini of uPA and uPAR were terminated by NH_3^+ and COO^-, respectively. To accurately replicate the state of the uPA–uPAR complex existing on the surface of a cancer cell, we added solvating water molecules in an 8 Å shell around the complex and considered them explicitly in our calculations. This solvated structure was optimized using the classical molecular mechanics (MM) program AMBER9 [20], in which the Parm99 [21] and TIP3 [22] force fields were used for the uPA–uPAR structure and the water molecules, respectively. The threshold value of the energy-gradient for the convergence of the AMBER9 optimization was set to 0.001 kcal/mol/Å.

2.2. Ab initio FMO calculations for the solvated uPA–uPAR complex

The solvated structure of uPA–uPAR has approximately 2600 water molecules, so it is not practical to calculate its electronic properties using the *ab initio* MO method. We thus considered only the solvating water molecules existing within 5 Å from amino acid residues 17–41 of uPA and amino acid residues 24–70, 122–171 of uPAR. In the previous experiment [12], these amino acid residues were found to contribute to the specific interactions between uPA and uPAR. This solvated uPA–uPAR complex has 436 water molecules.

To investigate the binding energy between uPA and uPAR, the solvated uPA–uPAR structure was divided into the following four structures.

1. uPA–uPAR complex containing solvating water molecules (complex).
2. uPA containing solvating water molecules (uPA + water).
3. uPAR containing solvating water molecules (uPAR + water).
4. Solvating water molecules (water).

From the total energies (T.E.) obtained from the FMO calculations, the binding energy (B.E.) between uPA and uPAR mediated by water molecules was estimated as

$$\text{B.E.} = -\text{T.E.(Complex)} + \text{T.E.(uPA + water)} + \text{T.E.(uPAR + water)} - \text{T.E.(water)}.$$

It must be noted that the basis set superposition error was neglected in the analysis of the binding energy between uPA and uPAR.

For the FMO [14–17] calculations, we used the ABINIT-MP program [23] developed by Nakano et al. The MP2 [24,25] method and the 6-31G basis-set were employed in the FMO calculations. One of the advantages of FMO is that FMO can obtain the interaction energies between the fragments using one SCF calculation while considering the effect of the surrounding fragments. This pair interaction energy obtained by FMO is somewhat similar to the simple pair interaction energy computed by classical force field methods. However, in the FMO evaluation of the pair interaction energy, the influence of the other fragments is taken into account as a direct coulomb interaction. In the present study, the fragment size was set as one amino acid residue or one water molecule. We thus investigated the interaction energies between each amino acid residue of uPA and uPAR, to elucidate which amino acid residues are important for the binding between uPA and uPAR. The effect of solvating water molecules on the specific interactions between uPA and uPAR was also investigated.

In addition, to analyze the effect of uPA amino acid residues on the specific interactions between uPA and uPAR, some of the important residues in uPA were mutated to other uncharged amino acids, and the solvated structure of the mutated uPA–uPAR complex was optimized using the classical MM method in AMBER9. For the optimized structure, the specific interactions between the mutated uPA and uPAR were investigated using the FMO method to determine the effect of the mutations on the interactions. From these computed results, we clarified which amino acid residues of uPA are

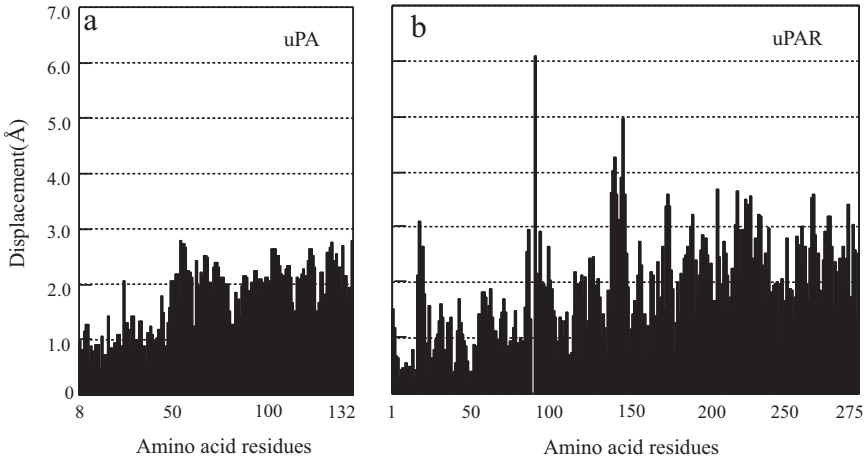

Fig. 1. Displacement of position for each Cα atom between the optimized and the experimental [19] structures for (a) uPA and (b) uPAR in the uPA–uPAR complex.

important for the binding interaction between uPA and uPAR. In the present study, we mutated the residues Lys23, Phe25, Lys46 and Lys98 in uPA. The Lys residues were mutated to uncharged Leu residues, while Phe25 was mutated to a simple Gly residue.

In principle, it is necessary to average interaction energies over all energetically accessible structures of the uPA–uPAR complex to derive experimentally relevant interaction energies. However, the FMO calculation for a single structure of the solvated uPA–uPAR takes several weeks using our computers, and the FMO calculations for many structures are so time-consuming task that we cannot finish the calculations within a realistic period of time. Therefore, we performed FMO calculations for the structure optimized by the classical MM method in AMBER9.

3. Results and discussion

3.1. Stable structure of the solvated uPA–uPAR complex

To verify the validity of the structure for the uPA–uPAR complex obtained by SWISS-MODEL [19], we compared it with the experimental model with PDB ID 3BT1[18]. The root mean square deviation (RMSD) between the structure generated with SWISS-MODEL and the experimental structures, for all amino acid residues except for the missing residues of uPAR, is 0.3 Å. Thus, we confirmed that the uPA–uPAR structure obtained using SWISS-MODEL [19] is comparable with the experimentally derived structure.

Furthermore, we verified the validity of the solvated structure of the uPA–uPAR complex optimized using the classical MM method of the AMBER9 program [20] with solvating water molecules considered explicitly. The RMSD for Cα atoms between the optimized and the experimental [18] structures is 2.0 Å. To clarify the reason for this large RMSD value, we investigated the displacement of position for each Cα atom between the optimized and the experimental uPA–uPAR structures. As shown in Fig. 1, the displacement is greater than 4 Å for amino acid residues 85, 130–131 and 136 of uPAR. Residue 85 exists near the missing residues (the 83rd and 84th) in the experimental structure, so which may be the reason this residue has a different positions. Amino acid residues 130–131 and 136 of uPAR exist on the surface of the uPA–uPAR complex. It is possible that these residues are affected by the solvation calculations, which have generated different positions from those observed in the X-ray crystal structure. Most of the Cα atoms with large displacements are on the surface of the complex. Accordingly, the large RMSD value observed between the optimized structure of the solvated uPA–uPAR and the X-ray crystal structure [18] of uPA–uPAR seems to be generated mainly from the solvation considered in the present study. We employed this solvated structure of uPA–uPAR complex in the *ab initio* FMO calculations.

3.2. Specific interactions between uPA and uPAR

To quantitatively elucidate the binding affinity between uPA and uPAR, the binding free energy should be evaluated. However, it is not practical to calculate free energies for the solvated uPA–uPAR complex using the *ab initio* FMO method. In the present study, we investigated the binding energies between uPA and uPAR and estimated the binding affinity qualitatively, on the assumption that the entropic effects on uPA, uPAR and uPA–uPAR are similar. In these analysis, we used the MP2/6-31G method of the ABINIT-MP [23] program with solvating water molecules considered explicitly. The results obtained by the present study are compared with those from our previous study [13] in Table 2, in which the total energies for the each part of the solvated uPA–uPAR complex are listed. The binding energies (B.E.) between uPA and uPAR estimated from these total energies are larger than 1000 kcal/mol for both structures. This large B.E. primarily comes from the electrostatic interactions between the charged amino acid residues of uPA and uPAR. In the present study, we considered solvating/hydrating water molecules explicitly and calculated the electronic states of the solvated uPA–uPAR complex in a vacuum. As a result, electrostatic interactions between the charged residues were estimated to be 80 times as large as those in water. In our previous FMO study

Table 2
Total energies (T.E.) for the solvated uPA–uPAR complex and each component of the uPA–uPAR complex, and the binding energy (B.E.) between uPA and uPAR estimated as B.E. = −T.E.(Complex) + T.E.(uPA + water) + T.E.(uPAR + water) − T.E.(water). The result obtained in our previous study [13] based on the other PDB structure (PDB ID: 2I9B) is listed for comparison.

PDB ID	Total energy (kcal/mol)				B.E. (kcal/mol)
	Complex	uPA + water	uPAR + water	Water	
3BT1	−126278469.2	−53956121.9	−93149044.2	−20827925.1	1228.2
2I9B	−113835371.9	−40153555.9	−81370227.6	−8406197.9	1187.1

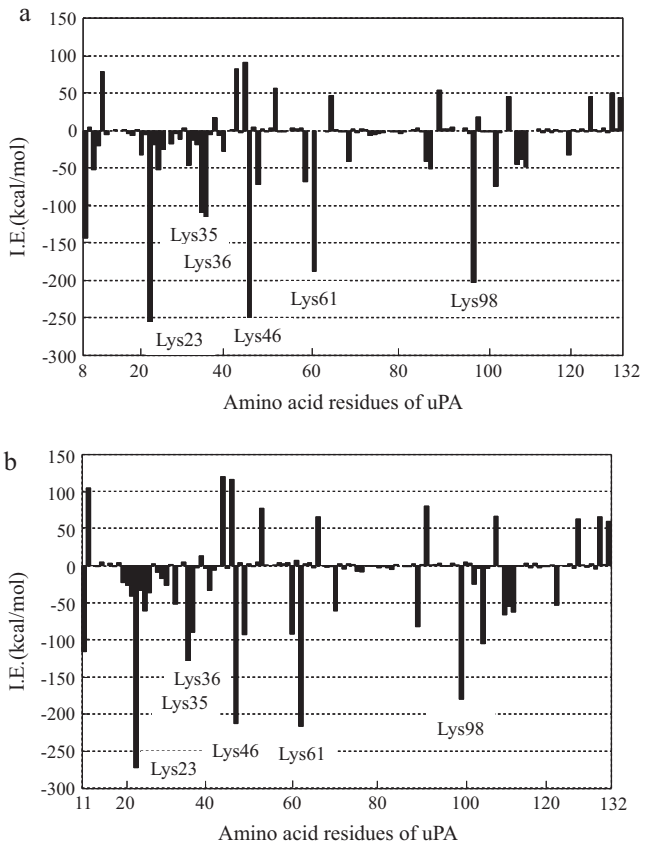

Fig. 2. Total of interaction energies (I.E.) between each amino acid residue of uPA and uPAR in the uPA–uPAR complex optimized in (a) the present and (b) the previous study [13].

[26] for the ligand–protein complex, the binding energies between ligand and protein evaluated in a vacuum are between 100 kcal/mol and 200 kcal/mol. In the uPA–uPAR complex, there are a large number of electrostatic interactions between the residues of uPA and uPAR. As a result, the B.E. between uPA and uPAR becomes larger. The B.E. for the structure obtained from the 3BT1 PDB structure is approximately 40 kcal/mol larger than that calculated for the previously obtained structure [13], indicating that the current structure is more stable than the previous structure.

To clarify which amino acid residues of uPA are important for the strong binding observed between uPA and uPAR, we investigated the interaction energies between each residue of uPA and all residues of uPAR. As shown in Fig. 2(a), the positively charged residues Lys23, Lys46, Lys98 and Lys61 of uPA have strong attractive interactions with uPAR, while the negatively charged residues Glu43, Asp45 and Asp12 of uPA have repulsive interactions with uPAR. These results come from the fact that uPAR is negatively charge as a whole. To confirm the reliability of the above results, we performed the same investigation for the uPA–uPAR structure obtained in our previous study [13]. As shown in Fig. 2(b), the important residues observed for uPA are the same as those in Fig. 2(a), although the strength of some interactions is different between the two models. Therefore, the above mentioned charged residues in uPA are confirmed to contribute significantly to the binding between uPA and uPAR. These results cannot be reached by using classical force fields because charge redistribution around the contact domain between uPA and uPAR in the uPA–uPAR complex cannot be considered in the classical force fields.

As shown in Fig. 2(a) and (b), Lys23 of uPA has the strongest attractive interaction with uPAR. To identify the reason for this strong interaction, we investigated in detail the interaction energies between Lys23 and each residue of uPAR. In Table 3, the residues having strong attractive interactions with Lys23 are listed in the decreasing order based on the strength of their interactions. Because Lys23 has positive charge, it interacts attractively with the negatively charged residues Asp and Glu of uPAR. In particular, there is a strong (−102.4 kcal/mol) attractive interaction between Lys23 and Asp140. To clarify the reason for this strong interaction, we evaluated the structure around these residues. As shown in Fig. 3, Lys23 is hydrogen bonded to the side chain of Asp140 with distances of 1.87 Å and 2.94 Å. In addition, the amino group at the end of the Lys23 side chain forms two hydrogen bonds, one with the OH group of the Thr127 side chain and one with the side chain of His166, whose bond lengths are 1.82 Å and 1.90 Å, respectively. As a result, Lys23 has large attractive interaction energies with Thr127 and His166, as indicated in Table 3. Consequently, it can be seen from Table 3 and Fig. 3 that the specific interactions between Lys23 of uPA and Asp140, Thr127 and His166 of uPAR are important for the binding between uPA and uPAR.

Table 3
Interaction energies (I.E.) (kcal/mol) between Lys23 of uPA and the amino acid residues of uPAR, which are listed in decreasing order of magnitude of energy.

Amino acids	I.E.
Asp140	−102.4
Thr127	−58.2
His166	−39.1
Glu173	−31.5
Asp254	−30.4
Asp124	−30.3
Asp163	−27.0
Asp141	−25.1
Glu106	−22.9
Glu134	−22.5

The previous experimental study [12] demonstrated that the hydrogen atom of the N-terminus of Lys23 and the oxygen atom of the side chain of Asp140 in uPAR are hydrogen bonded, and that the amino group of Lys23 is hydrogen bonded with the oxygen atom of the Thr127 side chain. The present computed results shown in Fig. 3 and Table 3 can explain this experimental result [12] at an electronic level.

It was also elucidated by previous experiments [10,11] that amino acids residues 19–31 of uPA make large contributions to the binding between uPA and uPAR. In addition, a systematic mutational analysis [27] revealed that Lys23, Tyr24, Phe25, Ile28 and Trp30 of human uPA are important for binding. We thus investigated the interaction energies between these residues of uPA and uPAR. As listed in Table 4, Lys23 has the largest (−262.4 kcal/mol)

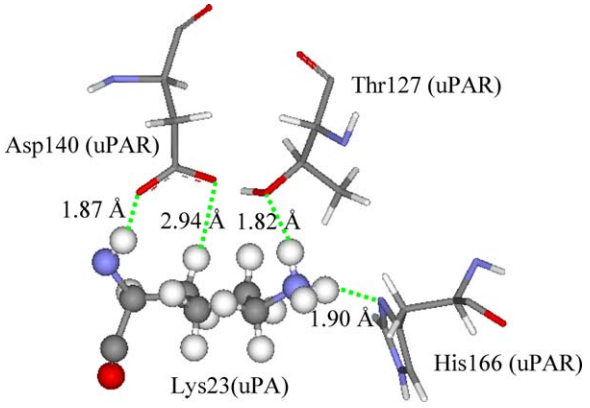

Fig. 3. Hydrogen bonding structures and distances (Å) between Lys23 of uPA and some amino acid residues of uPAR.

Table 4
Interaction energies (I.E.) (kcal/mol) between the amino acids from the 19th to 31st residues of uPA and uPAR.

Amino acids	I.E.
Cys19	−6.3
Val20	0.8
Ser21	−32.3
Asn22	−5.6
Lys23	−262.4
Tyr24	−18.5
Phe25	−52.3
Ser26	−25.0
Asn27	−0.5
Ile28	−17.1
His29	−4.6
Trp30	−12.1
Cys31	3.0

attractive interaction energy to uPAR among these residues. In addition, Phe25 has a large (−52.3 kcal/mol) interaction energy to uPAR. This interaction is between the oxygen atom of the Phe25 main chain and the positively charged Arg53 and Lys50 residues of uPAR. It is noted that the oxygen atom of the Phe25 main chain can attractively interact with the positively charged residues of uPAR, while the uncharged side chain of Phe25 has no electrostatic interaction to the charged amino acids in uPAR. There is no stacking interaction between the Phe25 side chain and the residues of uPAR in the solvated uPA–uPAR complex. An extensive surface plasmon resonance study [28] demonstrated that Phe25 significantly contributes to the human uPA–uPAR binding. Accordingly, it is concluded that among the amino acids residues 19–31 of uPA, Lys23 and Phe25 are important for the binding between uPA and uPAR.

In addition to the Lys23 and Phe25 residues of uPA, the other positively charged Lys residues of uPA have strong attractive interactions to uPAR, as shown in Fig. 2. There are 33 negatively charged residues (10 Asp and 23 Glu residues) and 28 positively charged residues (18 Arg and 10 Lys residues) in uPAR, so that the total charge of uPAR is estimated as −5. As a result, the positively charged residues of uPA have attractive interactions with uPAR. To clarify the effect of these residues on the uPA–uPAR interaction, we investigated the interaction energies between Lys or Arg residue of uPA and uPAR. As indicated in Table 5, Lys23, Lys46, Lys98, Lys61, Lys36 and Lys35 of uPA have attractive interaction energies with uPAR greater than −100 kcal/mol. In addition, as shown in Fig. 4, Lys35, Lys36, Lys46 and Lys61 of uPA are located near each other at a position near to the domain of uPAR that is composed of the negatively charged residues Glu33, Glu34, Glu36 and Glu37. Therefore, the results presented in Table 5 and Fig. 4 indicate that the electrostatic interactions between these positively charged residues of uPA and the negatively charged residues of uPAR contribute to the strong binding between uPA and uPAR.

Table 5
Interaction energies (I.E.) (kcal/mol) between the positively charged amino acid residues of uPA and uPAR.

Amino acids	Total of I.E.
Lys23	−262.4
Lys35	−109.0
Lys36	−119.6
Lys46	−249.6
Lys48	−71.6
Arg59	−68.5
Lys61	−187.6
Arg69	−41.5
Arg88	−50.4
Lys98	−202.6
Arg103	−73.8
Arg108	−45.1
Arg109	−38.2
Arg110	−48.6
Lys120	−32.1

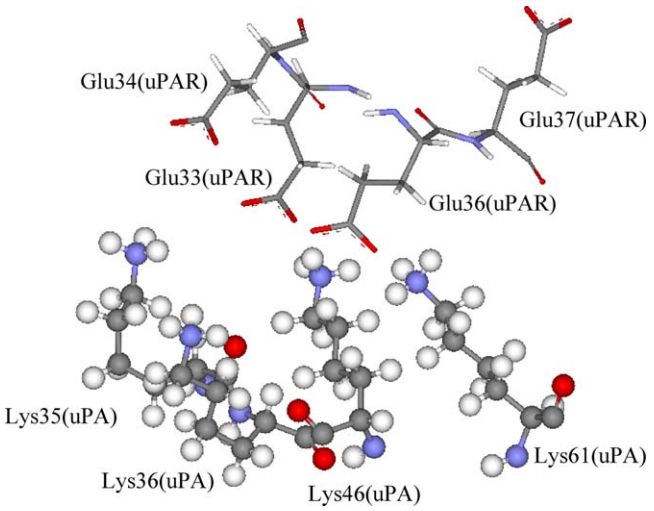

Fig. 4. Relative configurations of the positively charged Lys residues of uPA and the negatively charged Glu residues of uPAR.

Fig. 2 indicates that Lys46, Lys98 and Lys61 of uPA have strong attractive interactions with uPAR. These residues exist apart from residues 19–31 of uPA, which were considered important in the previous experiment [10,11]. To elucidate the contribution of these Lys residues to the uPA–uPAR interaction, we investigated their interaction energies with each residue of uPAR. The result for Lys46, which has the second-largest interaction energy with uPAR, is listed in Table 6(a). Lys46 has attractive interactions with the negatively charged Glu and Asp residues of uPAR. In particular, as shown in Fig. 5(a), the hydrogen atom at the end of the Lys46 side chain is hydrogen bonded to the oxygen atoms in the carboxylate groups of the Glu36 and Glu33 residues of uPAR. These hydrogen bonds produce the large attractive interaction energies between Lys46 and Glu36/Glu33, which are −117.0 kcal/mol and −108.6 kcal/mol, respectively. Lys61 of uPA also has a strong attractive interaction with uPAR. In particular, Lys61 interacts strongly (−111.3 kcal/mol) with Glu36 of uPAR, as indicated in Table 6(b). This interaction comes from the strong hydrogen bond between a hydrogen atom at the end of the Lys61 side chain and an oxygen atom of the Glu36 side chain, as shown in Fig. 5(b). The length of this hydrogen bond is 1.70 Å.

As for Lys98 of uPA, Table 6(c) indicates a strong attractive interaction (−122.9 kcal/mol) between Lys98 and Glu39 of uPAR. This strong interaction comes from the hydrogen bonds formed between the two hydrogen atoms of the amino group of the Lys98

Table 6
Interaction energies (I.E.) (kcal/mol) between (a) Lys46, (b) Lys61 and (c) Lys98 of uPA and each amino acid residue of uPAR, which are listed in decreasing order of magnitude of energy.

(a) Lys46		(b) Lys61		(c) Lys98	
Amino acids	I.E.	Amino acids	I.E.	Amino acids	I.E.
Glu36	−117.0	Glu36	−111.3	Glu39	−122.9
Glu33	−108.6	Glu34	−41.9	Leu40	−39.6
Glu34	−40.6	Glu33	−37.9	Glu37	−30.0
Asp102	−30.0	Glu37	−20.2	Glu42	−26.3
Glu37	−26.7	Asp102	−20.1	Glu36	−22.8
Asp141	−20.3	Glu39	−18.3	Glu68	−22.5
Glu39	−17.2	Asp141	−15.2	Glu15	−17.4
Glu106	−16.5	Asp140	−13.2	Glu33	−17.3
Asp140	−16.1	Glu120	−13.2	Asp140	−16.2
Glu94	−14.8	Glu42	−13.1	Glu120	−15.9

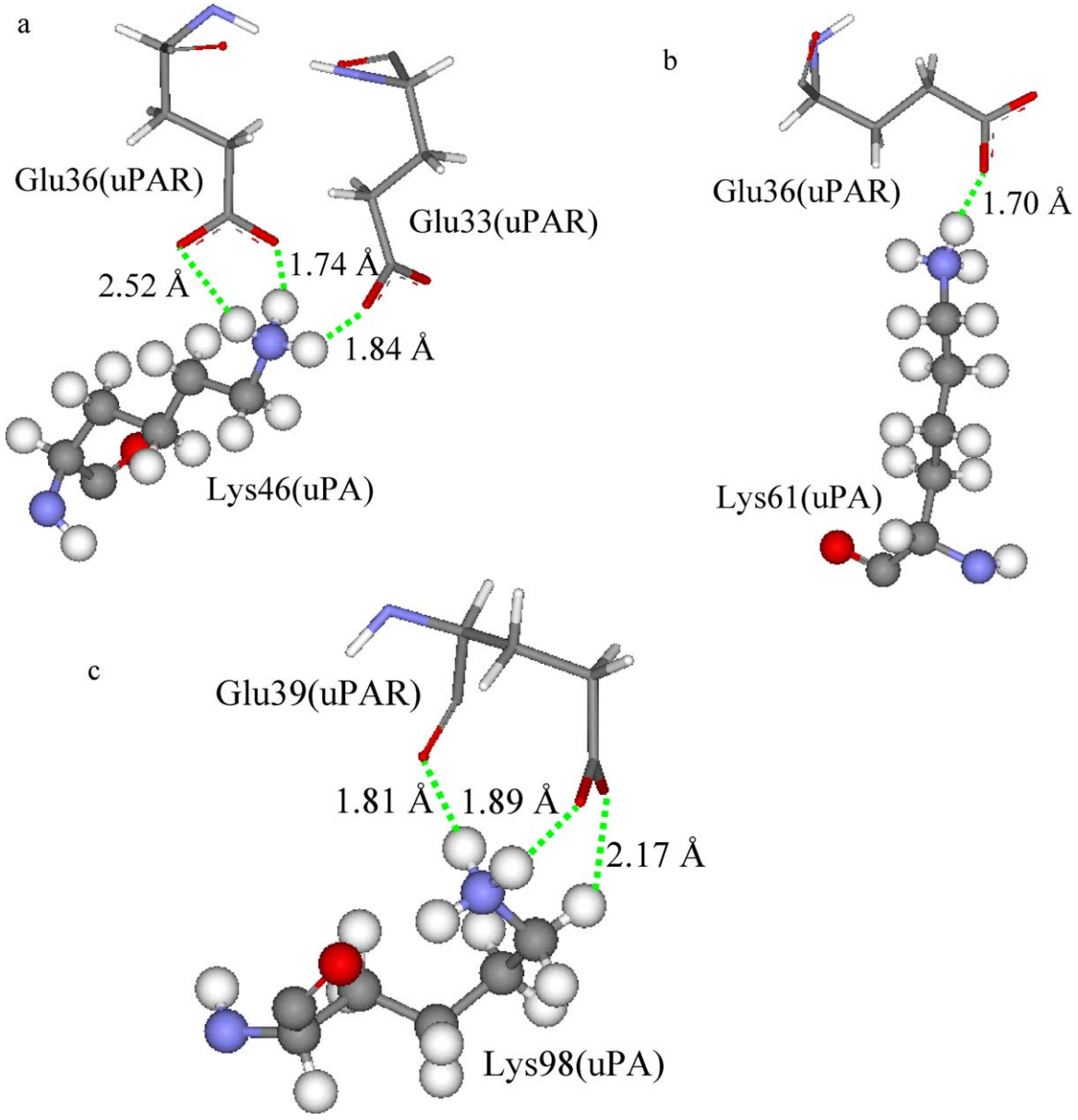

Fig. 5. Hydrogen bonding structures and distances (Å) between (a) Lys46, (b) Lys61, (c) Lys98 residues of uPA and some Glu residues of uPAR.

side chain and the oxygen atoms of Glu39, as indicated in Fig. 5(c). In contrast, a previous experiment [29] demonstrated that Lys98 of uPA is efficiently cross-linked to Lys43 of uPAR by a bifunctional crosslinker. In the present molecular simulations, we extract only the uPA and uPAR structures from the crystal structure of uPAR in complex with both the ATF of uPA and vitronectin because experiments [18] have indicated that there is no direct contact between uPA and vitronectin. To elucidate the effect of vitronectin on the structure of each amino acid residue in uPA–uPAR, we also investigated a stable structure for a solvated uPA–uPAR–vitronectin complex. The obtained structure indicates that the effect of vitronectin on the position of each amino acid residue in uPA–uPAR is at most 1 Å. Therefore, we did not consider vitronectin in the *ab initio* FMO calculations, which indicate that the positively charged residues Lys46, Lys61 and Lys98 in uPA are as important for the uPA–uPAR binding as the Lys23 and Phe25 residues of uPA.

As shown in Fig. 2, the residues Pro8 and Ala132 at the N- and C-terminus of uPA have large interaction energies, whose values are −144.0 kcal/mol and 43.4 kcal/mol, respectively. These large interactions come from the chemical groups of the N-terminus and C-terminus. In the present study, the N-terminus is terminated by NH_3^+, while the C-terminus is terminated by COO^-, so that Pro8 and Ala132 are positively and negatively charged, respectively. As a result, Pro8 has attractive interactions with the negatively charged Glu and Asp residues of uPAR, while Ala132 has repulsive interaction with these residues, as listed in Table 7. In what follows, we eliminate Pro8 and Ala132 of uPA from the list of residues contributing to specific interactions between uPA and uPAR.

3.3. The effect of solvating water molecules on the interaction between uPA and uPAR

In the present study, we considered solvating water molecules around the uPA–uPAR complex explicitly to accurately replicate the states of the uPA–uPAR complex on the surface of a cancer cell. From the computed electronic states for the solvated uPA–uPAR complex, it can be seen that several amino acid residues of uPA and uPAR interact through these solvating water molecules.

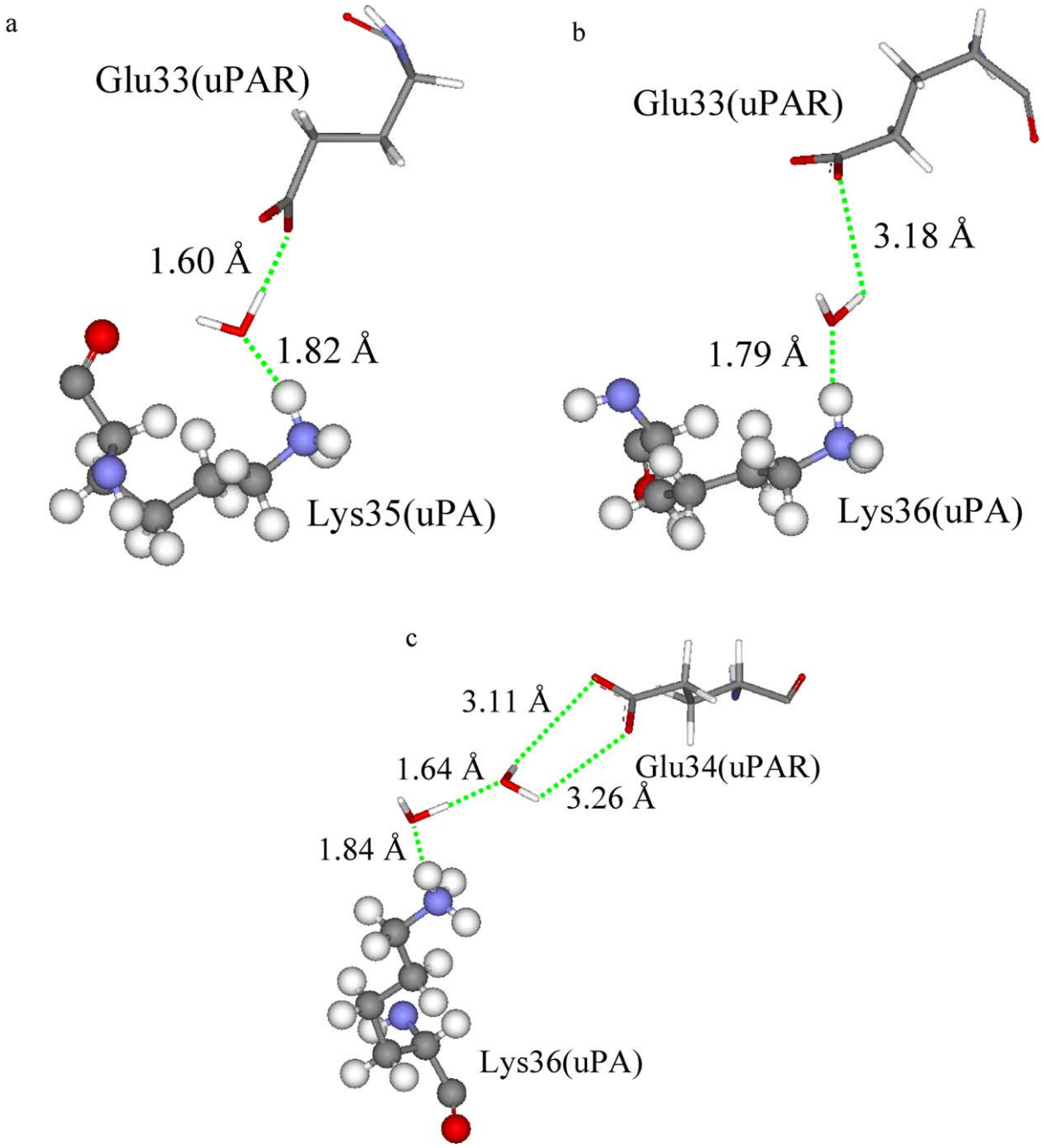

Fig. 6. Hydrogen bonding interactions and distances (Å) between the amino acid residues of uPA and uPAR bridged by water molecules; (a) between Lys35 of uPA and Glu33 of uPAR, (b) between Lys36 of uPA and Glu33 of uPAR, and (c) between Lys36 of uPA and Glu34 of uPAR.

Fig. 6(a) shows a hydrogen bonding interaction between Lys35 of uPA and Glu33 of uPAR via a water molecule. The water molecule forms strong hydrogen bonds with both the residues. The interaction energies between the water and Lys35 and Glu33 are −29.7 kcal/mol and −26.9 kcal/mol, respectively. Therefore, this water molecule bridges between the residues of uPA and uPAR using hydrogen bonds and enhances the interaction between uPA and uPAR. The other unique water molecule observed exists between Lys36 of uPA and Glu33 of uPAR, as shown in Fig. 6(b). The interaction energies between this water and Lys36 and Glu33 are −23.2 kcal/mol and −8.7 kcal/mol, respectively. This water molecule also contributes to the binding between uPA and uPAR.

In addition, we found a unique hydrogen bonding network between Lys36 of uPA and Glu34 of uPAR that is bridged by two water molecules, as shown in Fig. 6(c). One water molecule has a hydrogen bonding interaction (−18.1 kcal/mol) with Lys36, while the other water molecule has a hydrogen bonding interaction (−12.4 kcal/mol) with Glu34. Moreover, these two water molecules are hydrogen bonded to each other, with an energy of −13.1 kcal/mol. As a result, Lys36 and Glu34 interact through the two unique water molecules. The above investigations indicate the possibility that solvating water molecules existing between uPA and uPAR can significantly contribute to the specific interactions between uPA and uPAR. It should be noted that continuum solvation models cannot elucidate these interactions.

In our previous study [13] based on a different PDB structures, it was also demonstrated that there are some hydrogen bonding interactions between uPA and uPAR bridged by solvating water

Table 7
Interaction energies (I.E.) (kcal/mol) between (a) Pro8 and (b) Ala132 of uPA and each amino acid residue of uPAR, which are listed in decreasing order of magnitude of energy.

(a) Pro8		(b) Ala132	
Amino acids	I.E.	Amino acids	I.E.
Glu135	−65.4	Glu36	12.1
Glu132	−38.4	Glu34	11.5
Glu134	−30.3	Glu33	10.7
Asp141	−18.7	Asp102	9.1
Asp163	−18.0	Glu37	8.8
Asp120	−16.7	Glu39	8.8
Glu42	−16.7	Glu135	8.1
Glu183	−15.5	Asp141	8.0
Glu230	−14.6	Glu42	7.9
Asp102	−14.4	Glu106	7.3

molecules. Accordingly, these interactions are expected to occur often in the solvated uPA–uPAR complex. To confirm the existence of these interactions, long-time classical molecular dynamics simulations are currently underway for the solvated uPA–uPAR complexes. These results will make clear the influence of the thermal fluctuations of solvating water molecules on the specific interaction between uPA and uPAR.

3.4. The effect of amino acid substitutions on the interaction between uPA and uPAR

As mentioned in Section 3.2, Lys23, Phe25 and other Lys residues of uPA were found to be important for the binding between uPA and uPAR. To clarify the influence of these uPA residues on the uPA–uPAR interaction, we mutated these residues and optimized the solvated structure of the complexes formed between the mutated uPA and uPAR. Furthermore, the interaction energies between the mutated uPA and uPAR were investigated for the optimized structures. In the present study, we mutated residues Lys23, Phe25, Lys46 and Lys98 in uPA. The Lys residues were mutated to Leu, which is uncharged and has a similar side chain structure, while Phe25 was mutated to a simple Gly residue. The positions of these mutated residues are shown in Fig. 7, showing that Lys23 and Phe25 are located near the bottom of the central ligand-binding cavity of uPAR, while Lys46 and Lys98 bind specifically to uPAR residues around the rim of the cavity.

To elucidate the effect of the mutations on the binding affinity between uPA and uPAR, we first investigated the binding energies between the mutated uPA and uPAR using the FMO method. Table 8 lists the computed total energies for the uPA–uPAR complexes and their component structures, and the estimated binding energies between the mutated uPA and uPAR for the four types of mutations, indicating that the binding energy is reduced remarkably by all mutations. In particular, mutating Lys46 or Lys98 causes a large reduction in the binding energy. Therefore, from the view point of binding energy between uPA and uPAR, Lys46 and Lys98, which are located around the rim of the ligand-binding cavity of uPAR, are more important for the uPA–uPAR binding than Lys23

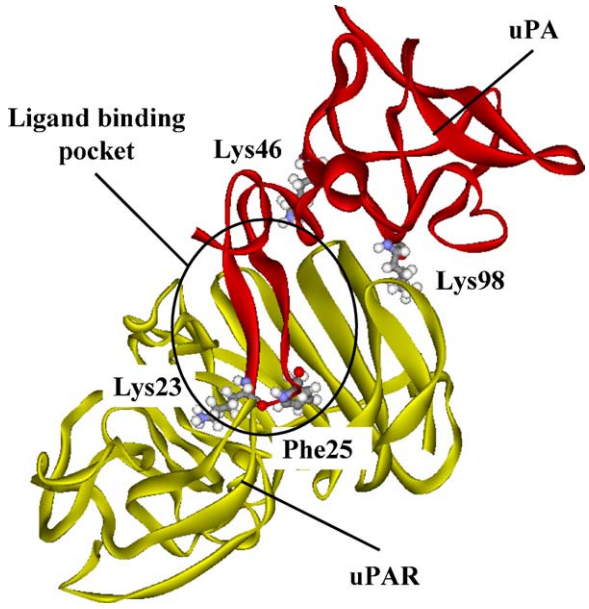

Fig. 7. A stable structure of the solvated complex with uPA and uPAR obtained by the present study. The solvating water molecules are not shown for clarifying the structure of the complex. The side chains of the important residues of uPA for the uPA–uPAR binding are shown to clarify their positions.

that is located in the ligand binding pocket. The effect mutating the uncharged Phe25 residue is much smaller than the effects of the Lys mutations.

To elucidate the origin of the change in binding energy induced by the mutations, we investigated the interaction energies between each residue of the mutated uPA and uPAR. The change in interaction energies is shown in Fig. 8 for the mutations. As shown in Fig. 8(a), the attractive interaction between Lys23 and uPAR is largely reduced by the Lys23Leu mutation. In contrast, the interaction energies between uPAR and residues Asn22 and Tyr24 of uPA are enhanced by 15 kcal/mol and 40 kcal/mol respectively. This enhancement comes from the creation of hydrogen bonds between residues Ser21, Asn22 and Tyr24 of uPA and residues Asp140, Lys50 and His166 of uPAR.

As shown in Fig. 8(b), the Lys46 mutation causes a large reduction in the attractive interaction between Lys46 and uPAR. In addition, the interaction between Cys11 and uPAR is strengthened because a hydrogen bond is created between the oxygen atom of the Cys11 backbone and a hydrogen atom of Lys139 in uPAR. In contrast, the repulsive interaction between Lys35 and uPAR is enhanced because the distance between Lys35 and Lys62 of uPAR is shortened by the mutation.

The mutation of Lys98 in uPA has a remarkable effect only on the interaction between Lys98 and uPAR, as shown in Fig. 8(c). The interaction energies between the other residues of uPA and uPAR are not changed significantly. The effect of the Phe25 mutation is shown in Fig. 8(d). Interactions between Asn22, Lys35, Lys36 and

Table 8
Total energies (T.E.) for the solvated uPA–uPAR complexes and their component structures, and the binding energies (B.E.) between uPA and uPAR estimated as B.E. = −T.E.(Complex) + T.E.(uPA + water) + T.E.(uPAR + water) − T.E.(water). The results for the four types of the mutated uPAs as well as the wild type uPA are listed.

Mutation	Total energy (kcal/mol)				B.E. (kcal/mol)
	Complex	uPA + water	uPAR + water	Water	
Wild type	−126278469.2	−53956121.9	−93149044.2	−20827925.1	1228.2
Lys23Leu	−126243636.8	−53921367.3	−93149161.5	−20827996.4	1104.5
Lys46Leu	−126243477.4	−53921354.2	−93148952.6	−20827853.1	1023.7
Lys98Leu	−126243518.9	−53921529.9	−93148991.6	−20828051.6	1049.1
Phe25Gly	−126109533.3	−53787232.6	−93149050.3	−20827950.2	1200.6

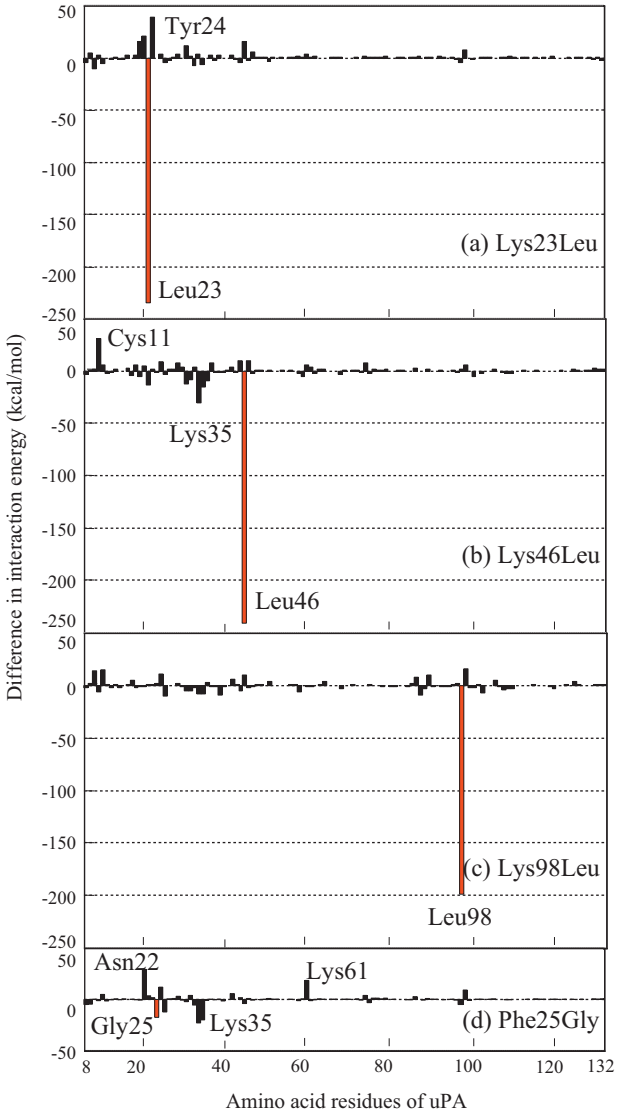

Fig. 8. Change in interaction energies between each amino acid residue of uPA and uPAR induced by the amino acid mutations of uPA; (a) Lys23Leu, (b) Lys46Leu, (c) Lys98Leu and (d) Phe25Gly mutations.

Lys61 of uPA and uPAR are affected by the mutation. The interaction between Asn22 and uPAR is 30 kcal/mol enhanced by the creation of hydrogen bond between Asn22 and Asp140 of uPAR. The change in interaction energies between Lys35, Lys36 and Lys61 and uPAR are less than 30 kcal/mol. Therefore, the effect of the Phe25 mutation is found to be much smaller than the effects from mutating the charged Lys residues.

Based on the computed results for the complexes between the mutated uPA and uPAR, we would propose two types of amino acid peptides that could bind specifically to the ligand binding cavity of uPAR and inhibit the interaction between uPA and uPAR. One peptide is composed of Lys23 and three residues upstream and downstream, which is expected to bind specifically to the bottom of the ligand-binding cavity of uPAR. The other peptide is composed of Lys46, Lys98 and residues between them from uPA. As shown in Fig. 7, Lys46 and Lys98 bind to the uPAR residues located near the rim of the ligand-binding cavity of uPAR, so a peptide composed of Lys46, Lys98 and a short amino-acid chain connecting them is expected to bind strongly to uPAR, to cover the ligand-binding cavity of uPAR and inhibit the entry of uPA into the cavity.

4. Conclusions

To elucidate the effects of mutating amino acids in uPA on the specific interaction between uPA and uPAR, we obtained stable structures of the solvated complexes between uPA (wild-type and mutated) and uPAR using the classical MM optimization and investigated the electronic states of the optimized structure using the FMO method. From the results computed by both the present and our previous [13] studies, the following points regarding the specific interactions between uPA and uPAR were elucidated.

(1) Positively charged Lys23 of uPA has the largest interaction energy with uPAR due to the hydrogen bonding interactions formed with Thr127 and Asp140 of uPAR.
(2) Positively charged Lys46, Lys98 and Lys61 have strong attractive interactions with negatively charged uPAR.
(3) Among the uncharged residues in uPA, Phe25 has the strongest attractive interaction with uPAR, due to the hydrogen bond formed between the oxygen atom of the Phe25 backbone and uPAR.
(4) The residues Lys46 and Lys98 of uPA located near the rim of the ligand-binding cavity of uPAR, have more of an effect on the binding energy between uPA and uPAR than the residue Lys23 which is located at the bottom of the cavity.

Inhibitors or antagonists of the uPA–uPAR system may provide suitable targets for anti-cancer therapy, and could include antagonist peptides, monoclonal antibodies to prevent uPA binding to uPAR and gene therapy. A potent peptide antagonist of the uPA–uPAR interaction that has a high affinity for uPAR might inhibit cancer cell invasion and metastasis. Therefore, if we can produce a peptide with characteristics of Lys46, Lys61 and Lys98 in same positions as in the uPA–uPAR complex, this peptide would cover the ligand binding cavity of uPAR. These novel peptides are proposed based on the present computed results on the specific interactions between uPA and uPAR. The overall results suggest that these antagonist peptides warrant further evaluation for their uses *in vitro* and *in vivo* cancer therapy.

Acknowledgments

This work was supported in part by grants from the Iketani Science and Technology Foundation, the Tatematsu Foundation, the CASIO Science Promotion Foundation and the Toukai Foundation for Technology.

References

[1] H. Kobayashi, J. Gotoh, Y. Hirashima, M. Fujie, D. Sugino, T. Terao, Inhibitory effect of a conjugate between human urokinase and urinary trypsin inhibitor on tumor cell invasion in vitro, J. Biol. Chem. 270 (1995) 8361–8366.
[2] E. Ruoslahti, How cancer spreads, Sci. Amer. 9 (1996) 48–55.
[3] A.E. Baker, J.D. Leaper, The plasminogen activator and matrix metalloproteinase systems in colorectal cancer: relationship to tumour patholog, Eur. J. Cancer 39 (2003) 981–988.
[4] M.M. Skelly, A. Troy, M.J. Duffy, H.E. Mulcahy, C. Duggan, T.G. Connell, D.P. O'Donoghue, K. Sheahan, Urokinase-type plasminogen activator in colorectal cancer: relationship with clinicopathological features and patient outcome, Clin. Cancer Res. 3 (1997) 1837–1840.
[5] L. Herszènyi, M. Plebani, P. Carraro, M. De Paoli, G. Roveroni, R. Cardin, Z. Tulassay, R. Naccarato, F. Farinati, The role of cysteine and serine proteases in colorectal carcinoma, Cancer 86 (1999) 1135–1142.
[6] J. Romer, B.S. Nilsen, M. Ploug, The urokinase receptor as a potential target in cancer therapy, Curr. Pharm. Des. 10 (2004) 2359–2376.
[7] H. Kobayashi, T. Terao, D. Sugino, M. Okushima, Cancerous metastasis inhibitor, United States Patent, 1997, WO97/25422.
[8] H. Sugiura, N. Tsumura, H. Kobayashi, N. Kurita, Electronic properties for medicine inhibiting cancer metastasis (1): molecular orbital calculations for physiological substance bikunin, J. Comput. Aided Chem. 5 (2004) 62–69.
[9] H. Sugiura, N. Tsumura, H. Kobayashi, N. Kurita, Electronic properties for medicine inhibiting cancer metastasis (2): molecular mechanics and molec-

ular orbital calculations for physiological substance bikunin, J. Comput. Aided Chem. 5 (2004) 70–76.
[10] E. Appella, E.A. Robinson, S.J. Ullrich, M.P. Stoppelli, A. Corti, G. Cassani, F. Blasi, The receptor-binding sequence of urokinase. A biological function for the growth-factor module of proteases, J. Biol. Chem. 262 (1987) 4437–4440.
[11] K. Bdeir, A. Kuo, B.S. Sachais, A.H. Rux, Y. Bdeir, A. Mazar, A.A. Higazi, D.B. Cines, The kringle stabilizes urokinase binding to the urokinase receptor, Blood 102 (2003) 3600–3608.
[12] C. Barinka, G. Parry, J. Callahan, D.E. Shaw, A. Kuo, K. Bdeir, D.B. Cines, A. Mazar, J. Lubkowski, Structural basis of interaction between urokinase-type plasminogen activator and its receptor, J. Mol. Biol. 363 (2006) 482–495.
[13] K. Nagase, E. Yoshikawa, H. Kobayashi, N. Kurita, Ab initio molecular orbital calculations on specific interactions between urokinase-type plasminogen activator and its receptor, J. Mol. Graph. Model. 28 (2009) 46–53.
[14] K. Kitaura, T. Sawai, T. Asada, T. Nakano, M. Uebayashi, Pair interaction molecular orbital method: an approximate computational method for molecular interactions, Chem. Phys. Lett. 312 (1999) 319–324.
[15] K. Kitaura, E. Ikeo, T. Asada, T. Nakano, M. Uebayashi, Fragment molecular orbital method: an approximate computational method for large molecules, Chem. Phys. Lett. 313 (1999) 701–706.
[16] T. Nakano, T. Kaminuma, T. Sato, Y. Akiyama, M. Uebayashi, K. Kitaura, Fragment molecular orbital method: application to polypeptides, Chem. Phys. Lett. 318 (2000) 614–618.
[17] T. Nakano, T. Kaminuma, T. Sato, K. Fukuzawa, Y. Akiyama, M. Uebayashi, K. Kitaura, Fragment molecular orbital method: use of approximate electrostatic potential, Chem. Phys. Lett. 351 (2002) 475–480.
[18] Q. Huai, A. Zhou, L. Lin, A.P. Mazar, J. Callahan, D.E. Shaw, B.C. Furie, M. Huang, Crystal structures of two human vitronectin, urokinase and urokinase receptor complexes, J. Nat. Struct. Mol. Biol. 15 (2008) 422–423.
[19] T. Schwede, J. Kopp, N. Gues, M.C. Peitch, SWISS-MODEL: an automated protein homology-modeling server, Nucleic Acids Res. 31 (2003) 3381–3385.
[20] D.A. Case, T.E. Cheatham III, T. Darden, H. Gohlke, R. Luo, K.M. Merz Jr., A. Onufriev, C. Simmerling, B. Wang, R.J. Woods, The AMBER biomolecular simulation programs, J. Comput. Chem. 26 (2005) 1668–1688.
[21] J. Wang, P. Cieplak, P.A. Kollman, How well does a restrained electrostatic potential (RESP) model perform in calculating conformational energies of organic and biological molecules? J. Comput. Chem. 21 (2000) 1049–1074.
[22] W.L. Jorgensen, J. Chandrasekhar, J. Madura, M.L. Klein, Comparison of simple potential functions for simulating liquid water, J. Chem. Phys. 79 (1983) 926–935.
[23] T. Nakano, et al., http://www.ciss.iis.u-tokyo.ac.jp/rss21/.
[24] Y. Mochizuki, T. Nakano, S. Koikegami, S. Tanimori, Y. Abe, U. Nagashima, K. Kitaura, A parallelized integral-direct MP2 method with fragment molecular orbital scheme, Theor. Chem. Acc. 112 (2004) 442–452.
[25] Y. Mochizuki, S. Koikegami, T. Nakano, S. Amari, K. Kitaura, Large scale MP2 calculations with fragment molecular orbital scheme, Chem. Phys. Lett. 396 (2004) 473–479.
[26] K. Dedachi, M.T.H. Khan, I. Sylte, N. Kurita, A combined simulation with ab initio MO and classical vibrational analysis on the specific interactions between thermolysin and dipeptide ligands, Chem. Phys. Lett. 479 (2009) 290–295.
[27] V. Magdolen, P. Rettenberger, M. Koppitz, L. Goretzki, H. Kessler, U.H. Weidle, B. Konig, H. Graeff, M. Schmitt, O. Wilhelm, Systematic mutational analysis of the receptor-binding region of the human urokinase-type plasminogen activator, Eur. J. Biochem. 237 (1996) 743–751.
[28] L. Lin, H. Gardsvoll, Q. Huai, M. Huang, M. Ploug, Structure-based engineering of species selectivity in the uPA–uPAR interaction: implication for preclinical cancer therapy, J. Biol. Chem. 285 (2010) 10982–10992.
[29] H. Gardsvoll, B. Gilquin, M.H.L. Du, A. Menez, T.J.D. Jorgensen, M. Ploug, Characterization of the functional epitope on the urokinase receptor, J. Biol. Chem. 281 (2006) 19260–19272.